Image Reconstruction of Metal Pipe in Electrical Resistance Tomography

**[1] Suzanna RIDZUAN AW, [2, 3, *] Ruzairi ABDUL RAHIM,
[2] Yusri MOHD YUNUS, [3] Mohd Hafiz FAZALUL RAHIMAN,
[4] Yasmin WAHAB, [2] Fazlul Rahman Mohd YUNUS,
[5] Elmy Johana MOHAMED, [6] Azian ABDUL AZIZ, [2] Chiew Loon GOH,
[2] Jayasuman PUSPPANATHAN, [7] R. G. GREEN and [8] Zhen Cong TEE**

[1] Faculty of Electrical & Automation Engineering Technology, TATiUC, Jalan Panchor,
Telok Kalong, Kemaman, Terengganu, 24000, Malaysia
[2] Process Tomography and Instrumentation Engineering Research Group (PROTOM-i), Innovative
Engineering Research Alliance, Faculty of Electrical Engineering, Universiti Teknologi Malaysia,
Johor, 81310, Malaysia
[3] School of Mechatronic Engineering, Universiti Malaysia Perlis, Pauh Putra Campus,
Arau, Perlis, 02600, Malaysia
[4] Department of Instrumentation & Control Engineering (ICE), Faculty of Electrical & Electronics
Engineering, Universiti Malaysia Pahang, Pekan, Pahang, 26600, Malaysia
[5] Department of Mechatronics and Robotics, Faculty of Electrical and Electronic Engineering,
Universiti Tun Hussein Onn Malaysia, Johor, 86400, Malaysia
[6] Language Academy, Universiti Teknologi Malaysia, Johor Bahru, 81310, Malaysia
[7] School of Engineering, Sheffield Hallam University, Sheffield, United Kingdom
[8] Logo Solution Sdn. Bhd. Johor, 81200, Malaysia
[2] Tel.: +60197104000, fax: +607-4537150
E-mail: ruzairi@fke.utm.my, ruzairi@uthm.edu.my

Abstract: This paper demonstrates a Linear Back Projection (LBP) algorithm based on the reconstruction of conductivity distributions to identify different sizes and locations of bubble phantoms in a metal pipe. Both forward and inverse problems are discussed. Reconstructed images of the phantoms under test conditions are presented. From the results, it was justified that the sensitivity maps of the conducting boundary strategy can be applied successfully in identifying the location for the phantom of interest using LBP algorithm. Additionally, the number and spatial distribution of the bubble phantoms can be clearly distinguished at any location in the pipeline. It was also shown that the reconstructed images agree well with the bubble phantoms.

Keywords: Conducting boundary strategy, Finite element method, Electrical resistance tomography, Linear back projection, Metal pipe.

1. Introduction

Tomography offers a unique opportunity to reveal the complexities of internal structure of an object without the need to invade the object. One of the most extensive modalities of tomography is the Electrical Resistance Tomography (ERT). ERT is an accepted diagnostic technique for imaging the interior of

opaque systems. It is relatively safe, inexpensive to operate and is relatively fast, thus enabling real-time monitoring of processes. This technique has found applications in many areas, including medical imaging, environmental monitoring, and industrial processes. Electrical Resistance Tomography (ERT) has become a promising technique in monitoring and analysing various industrial flows due to its diverse advantages, such as high speed, low cost, suitability for various sizes of pipes and vessels, having no radiation hazard, and being non-intrusive [1-3, 20, 21]. It provides cross sectional images of conductivity distribution within its sensing region. For a system employing ERT on a metallic or conducting vessel pipe, the electrodes need to be insulated from the pipe wall. In addition, the conducting boundary strategy needs to be applied to overcome the grounding effect [4, 5].

Since the ERT model is nonlinear and difficult to be solved analytically, the finite element method (FEM) is preferable in solving forward modeling. From the solution, the data is interpolated to generate the sensitivity distribution. Later, the sensitivity distribution obtained is used with linearized method to solve inverse problems.

In this paper, simulations were used in reconstructing the image of bubble phantoms in a metal wall using conducting measurement techniques in ERT. FEM was used to solve the forward model and the data obtained were then interpolated in MATLAB to obtain the sensitivity distribution for every possible injection-measurement electrode pair and the total sensitivity distribution. Then, every projected voltage measurements for both the homogeneous and nonhomogeneous systems were recorded. Lastly, an image reconstruction was developed using the Linear Back Projection (LBP) algorithm. Goals of the current research and development efforts involved verifying the feasibility and effectiveness of the sensitivity maps developed in reconstructing the image for the system under investigation.

2. System Configuration

Sixteen rectangular electrodes of 12 mm × 100 mm were utilized in this research. The electrodes were mounted at the center of a stainless steel column and evenly spaced along the circumference. The system was modelled in 2D planes using COMSOL Multiphysics 4.2®, a finite element analysis tool. The settings of the parameter used in the simulation are shown in Table 1. For an invasive ERT, the electrodes must be in continuous contact with the medium inside the column. Hence, in this research, it is assumed that the electrodes make electrical contact with the fluid inside the column but do not affect the normal mass transfer within the system.

A flexible circuit board was used as the electrode in the research. It is to be noted that metal electrodes for electrically-conducting (metallic) column differ slightly from a non-conducting (insulating) column in which the electrodes need to be insulated from the conducting column. Fig. 1 shows the design of the electrode fabrication using flexible circuit board of the proposed system for the ERT system deploying a conducting vessel.

Table 1. Simulation parameters with COMSOL 4.2a.

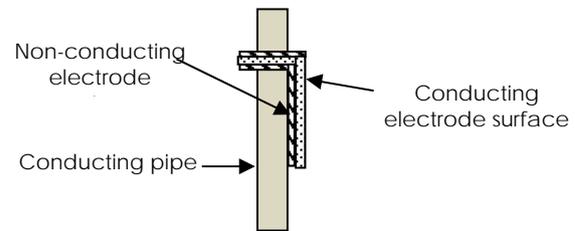| Parameter	Value
Column's Inner radius	50 mm
Column's Outer radius	51 mm
Column Height	300 mm
Number of electrodes (N)	16
Electrode's material	Gold
Insulator's material	FR4
Electrode's width (w) x height (h)	12×100 mm
Current excitation	5 mA
σ_{water}	8.3×10^{-3} S/m

Fig. 1. Electrode Fabrication using flexible circuit board.

A 2D physical model has been developed such that it mimics the real ERT system being developed in the laboratory for experimental purposes. Sixteen electrodes that were insulated from the column wall were placed equidistantly inside the column. The materials for each related domain in the model were defined such that they also resemble the real ERT system. The domain for the column was set to be of stainless steel material and the main medium inside the column was tap water with a conductivity of 8.3 mS/m. The electrodes utilized were from a flexible gold coated printed circuit board (PCB). FR4 material was chosen as the material for the insulating part of the electrodes. FR, which stands for Flame Retardant, is a glass fiber epoxy laminate that is most commonly used in PCB materials. All boundary and initial conditions were set to produce an electrical field, solving any electrical potential distribution. The cross section view of the COMSOL model is shown in Fig. 2.

For the ERT system that uses a metal pipe, the adjacent strategy, which is the most commonly used measurement method in ERT is unsuitable for application to the conducting vessel since much of the electrical current from the injection electrode would travel to the ground through the wall material rather than through the multiphase mixture. This greatly reduces the sensitivity of the system. This is called the grounding effect of the vessel. To overcome the grounding effect of the vessel, a conducting boundary strategy was implemented on the model. The strategy

involved each electrode acting sequentially as a current source whilst the whole of the conducting vessel behaved as a grounded current sink. This is illustrated in Fig. 3.
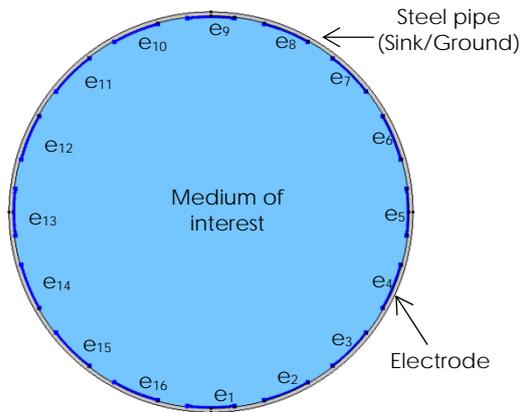

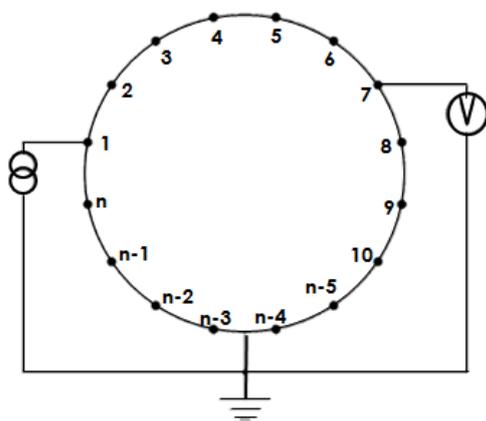**Fig. 2.** ERT Model using Metal Pipe.

Fig. 3. Conducting Boundary Strategy [6].

A constant current of 5 mA was injected initially at the source electrode, namely electrode 1, e1. In this strategy, all the voltage measurements were referenced to the same earth potential of the conducting boundary which is the pipe itself [7]. This procedure is repeated for all possible pairs of electrodes until a full rotation of the electrical field was obtained. The current density streamline when the metal pipe is grounded is shown in Fig. 4 resulting electrical field when one electrode acted as the source electrode and the others acted as the measurement electrodes, conditioned by the material distribution within the domain of interest is shown in Fig. 5.

3. Image Reconstruction

The sensing field of an ERT system is spread over the entire volume due to its "soft-field" characteristics [8-10]. The paths of electric currents in an ERT system are nonlinear. Current diffuses all over the target, and the current distribution depends on the material's internal conductivity distribution $\sigma = \sigma\,(r)$ [11]. The image reconstruction problem of conductivity distribution in ERT is an ill-posed and ill-conditioned inverse problem. To solve this inverse problem, a forward model that relates to the dependency between conductivity distribution and boundary voltages need to be solved first. The ERT tomogram, which is the cross sectional image is developed by solving the conductivity distribution in the area of interest.
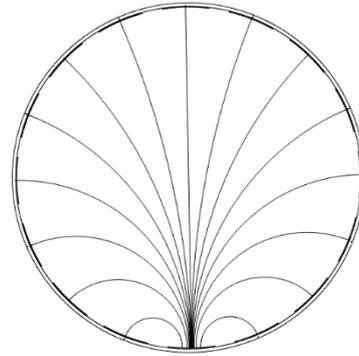

Fig. 4. Current Density Streamline of Metal Pipe using Conducting Strategy.
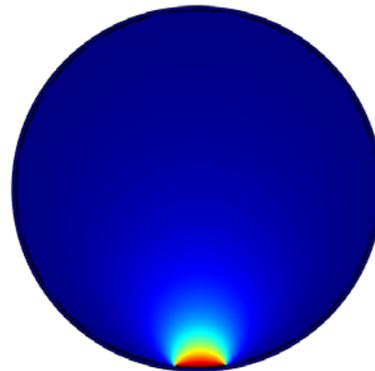

Fig. 5. Electrical Field for Single Injection Electrode.

3.1. Forward Problem

In ERT, the forward problem computes the electrical potentials in the boundary by utilising the initial estimation of the conductivity distribution. The forward problem can be represented by equation (1), where $Y, v,$ and c denote the global conductance matrix, the nodal voltage vector, and the nodal current vector respectively.

$$Y \cdot v = c \qquad (1)$$

Maxwell's law is used in this forward problem to model the distribution of the electrical field of the ERT system. The sensitivity distribution is solved in forward problems using the analytical approach. The sensitivity distribution of a homogeneous conductivity

medium can be acquired by solving the forward model using both analytical and numerical method. Since it is difficult to obtain the analytical solutions of the equation, the numerical solvers, i.e., the finite element methods (FEM) are preferable and the most commonly used method to solve the forward problem. COMSOL Multiphysics 4.2, has been utilized in this work to solve the forward problem of an ERT system of a conducting vessel pipe.

3.2. Sensitivity Distribution using Conducting Strategy

The sensitivity theorem or lead theorem which analysed the boundary of mutual impedance experienced by the changes of conductivity within the sensing region has been introduced by Geselowitz and later refined by Lehr. It is based on Green's theorem and the divergence theorem [12]. By adapting the two theorems to a conducting volume as shown in Fig. 6, the reciprocity theorem (Equation 2) and lead theorem of mutual impedance Z (Equation 3) can be deduced as [13]:

$$I_\phi \psi_{AB} = I_\psi \phi_{CD} \qquad (2)$$

$$Z = \phi_{CD}/I_\phi = \psi_{AB}/I_\varphi, \qquad (3)$$

where ψ_AB and ϕ_CD are the voltage potentials measured between terminal AB and CD due to the injection currents I_ψ and I_ϕ respectively. From the divergence and reciprocity theorem, Geselowitz and Lehr derived a relationship between the mutual impedance changes, ΔZ and the conductivity changes [14].

$$\Delta Z = \frac{\Delta \varphi_{CD}}{I_\varphi} = - \int_v \Delta\sigma \frac{\nabla\varphi}{I_\varphi} \cdot \frac{\nabla\psi}{I_\psi} dv \qquad (4)$$
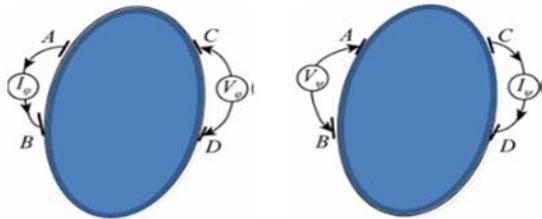

Fig. 6. Mutual Impedance Relation between Terminal AB and CD [15].

Solving for Equation 4, the sensitivity theorem to solve the inverse problem of ERT can be simplified to:

$$S_{ij} = \frac{\Delta R}{\Delta\sigma} = - \int_v \frac{\nabla\varphi_i}{I_i} \cdot \frac{\nabla\varphi_j}{I_j} dv \qquad (5)$$

where S_{ij} is the sensitivity distribution when the i-th and j-th electrode pair is in excitation and measurement respectively, R is the mutual resistance that is a special case of mutual impedance, Z, φ_i is the potential distributions within the medium when the i-th electrode is excited by current I_i, φ_j is the potential distributions within the medium when the j-th electrode is excited by current I_j.

Assuming that the conductivity distribution is composed of k small uniform pixels, the sensitivity coefficient of each pixel can be deduced as [15].

$$S_{i,j}(k) = - - \int_{\Omega_k} \frac{\nabla\varphi_{ik}}{I_i} \cdot \frac{\nabla\varphi_{jk}}{I_j} d\Omega_k, \qquad (6)$$

where Ω_k is the discrete 2D area of the k-th pixel, $s_{i,j}(k)$ is the sensitivity coefficient at the k-th pixel when the i-th and j-th electrode pairs are in excitation and measurement respectively, φ_{ik} is the potential distributions at the k-th pixel when the i-th electrode is excited by current I_i, φ_{jk} is the potential distributions at the k-th pixel when the j-th electrode is excited by current I_j.

The procedure of attaining the sensitivity distribution is only complete when all electrodes are used for injection, such that the cycle has all the possible projections. The sensitivity matrix can then be expressed by [15].

$$S = $$
$$= \begin{bmatrix} S_{1,2}(1) & S_{1,2}(2) & \cdots & S_{1,2}(k) & \cdots & S_{1,2}(M) \\ S_{1,3}(1) & S_{1,3}(2) & \cdots & S_{1,3}(k) & \cdots & S_{1,3}(M) \\ \vdots & \vdots & \cdots & \vdots & \cdots & \vdots \\ S_{i,j}(1) & S_{i,j}(2) & \cdots & S_{i,j}(k) & \cdots & S_{i,j}(M) \\ \vdots & \vdots & \cdots & \vdots & \cdots & \vdots \\ S_{n-2n}(1) & S_{n-2n}(2) & \cdots & S_{n-2n}(k) & \cdots & S_{n-2n}(M) \end{bmatrix}$$
$$(7)$$

The sensitivity theorem is also applicable to the conducting vessel because the electrical field within the vessel still obeys Greens' and the reciprocity theorem. Here, 128×128 pixels which equals to 16384 pixels is implemented to attain the sensitivity distribution. The electric potential, φ and the electric field distribution, E is governed by equation 8.

$$-\nabla\varphi = E \qquad (8)$$

Thus, Equation (8) that denotes the sensitivity of the electrode pair i-j (i for excitation and j for measurement) to the conductivity change in a pixel at position k-th can be rewritten as:

$$s_{i,j}(k) = \int_{\Omega k}(E_{ik}/I_i) \cdot (E_{jk}/I_j) d\Omega_k, \qquad (9)$$

where E_{ik} and E_{jk} are the electric field strength at k-th pixel when the i-th and j-th electrode pairs are injected with currents I_i and I_j respectively in turn[16]. Practically, it is assumed that the electric field is the same at every point of the area Ω_k since the pixels are so small. Assuming a unit current, Equation (9) can be deduced to equation 10.

$$s_{i,j}(k) = E_{ikc}.E_{jkc}A_{\Omega_k} \qquad (10)$$

where E_{ikc} and E_{ikc} are the electric field intensities at the centre of k-th pixel when the i-th electrode pair is in excitation mode and the j-th electrode pair is in measurement mode. A_{Ω_k} is the area of the k-th pixel. Finally, the sensitivity coefficient of each pixel is also obtained. The sensitivity coefficient for each electrode pair at a spatial location k-th is obtained by the dot product of the two electric fields. The sensitivity matrix is represented by the sensitivity map.

The sensitivity map for each configuration of electrode 1, showing the excitation of the ERT system that was fitted with 16 electrodes on a stainless steel pipe modelled in COMSOL is illustrated in Fig. 7.
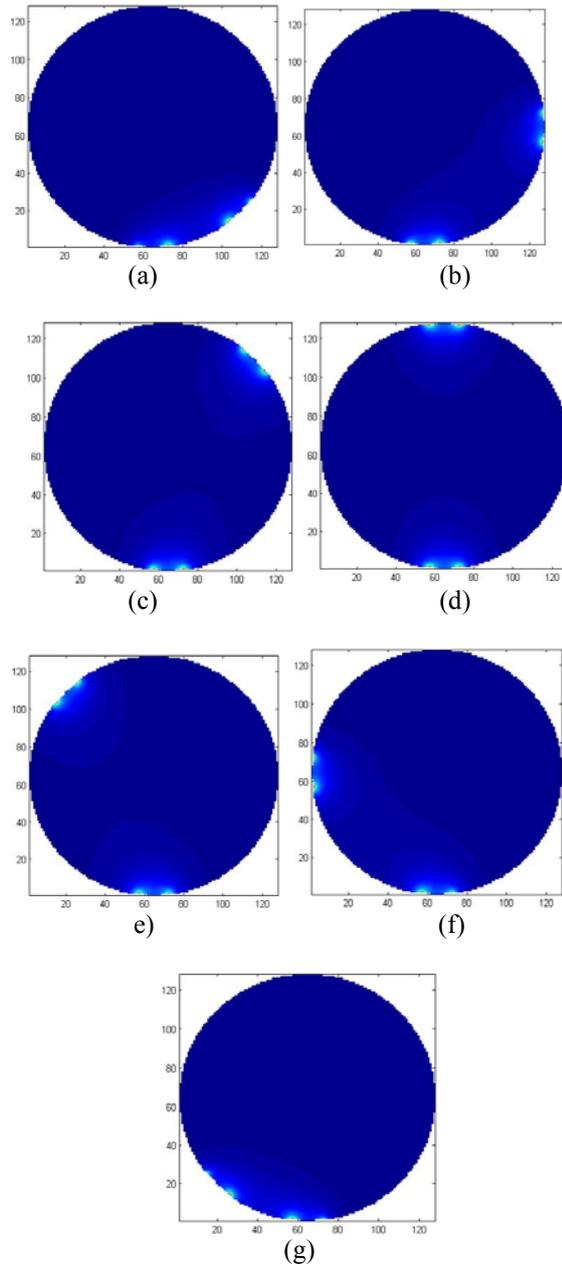
Fig. 7. Sensitivity Map Distribution of: (a) electrodes 1 and 3, (b) electrodes 1 and 5, (c) electrodes 1 and 7, (d) electrodes 1 and 9, (e) electrodes 1 and 11, (f) electrodes 1 and 13, (g) electrodes 1 and 15.

From the map, it is observed that the sensitivity field is non-uniformly distributed over the medium of interest. The sensitivity is higher within the area close to both excitation and measurement electrode pair. When it is away from the active injection electrode pair, the sensitivity is lower. The combination of all independent projection of the electrode pair configurations is as shown in Fig. 8. It is also known as the weight balance map (WBM).

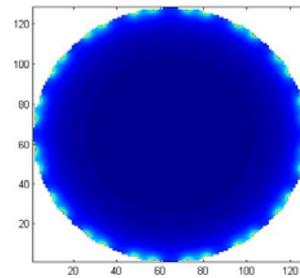The surface matrix of the WBM is as presented in Fig. 9 below.
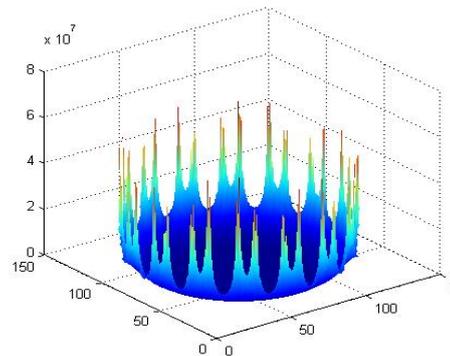

Fig. 8. Weight Balance Map.

Fig. 9. Surface Matrix of the WBM.

3.3. Inverse Problem

As for the inverse problem, the conductivity distribution is reconstructed based on the electric potentials measured in the boundary, through the use of an adequate mathematical procedure [17]. One needs to solve the forward problem for some assumed conductivity before solving the inverse problem, so that the expected voltages can be compared with the measured data. Furthermore, the interior electric fields are normally required for the calculation of a Jacobian. Typically, FEM is used to compute the boundary voltages for a known conductivity distribution. Only in cases of a very simple geometry, and homogeneous in nature, or at least with very simple conductivity, could the forward problem be solved analytically [18].

There are numerous methods to reconstruct the ERT images which can be broadly divided into three classes: linear (single step and iterative methods); non-linear iterative methods; and heuristic multivariate

methods. However, the linear method has been chosen in this research since it is the most quick and simple. The linear methods are fast since the images are produced by simply multiplying the measurements by a single, pre-calculated matrix. In the linear method, Linear Back Projection (LBP) is the most extensively applied by researchers. The matrix in LBP is the transposal of an estimated solution to the forward problem, based upon either field gradients or more commonly, sensitivity maps (where the area in the measuring volume is divided into sensitivity areas). LBP is known as the non-iterative linear method [17].

LBP algorithm is a type of back projection algorithm and is essentially based on the linearization of a normalized form of the original problem. The projection data from each sensor with its sensitivity maps is combined to generate a concentration profile in LBP. Theoretically, given by the corresponding sensitivity map, LBP can be viewed as a weighted back projected or "smearing" of each one of the normalized measurements along its sensing zone [19].

The principle of this back-projection in ERT is that a relative change of the boundary measurement, $\Delta V_{(i,j)}/V_{(i,j)}$ with its sensitivity at each pixel as its weight factor is back-projected to the whole domain as relative changes of the conductivity at each pixel in the i,j projection. Because of its linear approach and fixed weight factors, LBP could not provide an accurate image. Nonetheless, it provides a fast on- line view or preview for initial visualization [12].

3.3.1. Implementation of LBP

For the LBP implementation in this research, the first step was the calibration for a homogeneous system. The homogeneous flow for this research was a full flow of tap water with a conductivity of 8.33 × 10-3 S/m. Later, the system was used to reconstruct the cross-sectional image of the region of interest based on Equation 11 that represents the LBP algorithm.

$$BP\,(x,y) = \sum_{Tx=0}^{n} \sum_{Rx=0}^{n} A_{Tx,Rx} \times \bar{S}_{Tx,Rx}(x,y) \qquad (11)$$

where $LBP\,(x,y)$, is the profile showing the concentration image obtained using the LBP algorithm in $n \times n$ (128 × 128) matrix where n equals to the dimension of the sensitivity matrix; $\bar{S}_{Tx,Rx}(x,y)$ is the normalized sensitivity map for the view of transmitter Tx to receiver Rx, and $A_{Tx,Rx}$ is the sensor loss value which refers to the difference of the homogeneous and non-homogeneous flow for the projection of transmitter Tx to receiver Rx. Non-homogeneous flow refers to the flow condition when a phantom or object exists inside the pipe. $A_{Tx,Rx}$ is represented in Equation 12 below:

$$A_{Tx,Rx} = \frac{V_{homo}(Tx,Rx) - V_{non-homo}(Tx,Rx)}{V_{homo}(Tx,Rx)}, \qquad (12)$$

where $V_{homo}(Tx,Rx)$ is the electric potential measured when Tx acts as source electrode and Rx acts as the receiver electrode in the condition of full water flow; while $V_{non-homo}(Tx,Rx)$ is the electric potential measured when Tx acts as the source electrode and Rx acts as the receiver electrode in the condition of a non-homogeneous flow.

The algorithm is then applied in a programming environment along with the sensor loss data and sensitivity maps to be computed and programmed to generate the image. The authors used the MATLAB programming environment to reconstruct the image.

4. Results and Discussions

In the simulation of the two-phase flow model using COMSOL, the properties for each material under investigation are based on their real properties. Based on the sensor loss and sensitivity maps obtained, MATLAB was used to reconstruct the image diameter of bubble phantom placed close to each other.

From the results presented in Table 2, the reconstructed images produced successfully displayed the location of phantoms of interest correctly using the LBP algorithm. It is observed that the sensor loss value is higher when there is existence of an object in between the source electrode and receiver electrode. This causes the concentration profile to become higher and denser at the located object. For a single phantom, the location of the bubble image resembles the real location of the phantom.

As for the images when there exist more than one phantom such as illustrated in the 4th and 5th results, it is shown that LBP is still sufficient to produce the correct location of the image even though the shapes of the phantoms are not 100% accurate. This is caused by the smearing effect in LBP due to its linear approach and fixed weight factor. Bubbles located at the center of the pipe, could lead to artefacts in the image. When the bubble is located near the boundary of the pipe, the grounded wall will introduce much more artefact and blurring to the boundary or even distort the reconstructed image. Although it is proven that LBP is still adequate enough to be implemented for initial visualization and verification of the study, LBP is not good enough to obtain the image of bubbles which are located close to one another. The conductivity distribution changes too much when two bubbles are located too near to each other. The sensitivity values decreases when the excitation using LBP algorithm. A number of bubble phantoms were tested to justify the research. In order to verify the efficiency and feasibility of the research as well as the sensitivity based image reconstruction algorithm, the reconstructed image of six phantoms for the two-phase flow (water/gas) displayed in Table 2 were analyzed.

The first one shows the image acquired when a bubble phantom of 20 mm diameter was located at the center of the pipe. The second result is the image generated when a 20 mm diameter of bubble was

located at 90º. The third result shows the image of a phantom of bubble with 20 mm diameter located at 270º. Next, the image of two bubble phantoms of 20 mm diameter each was shown with the bubbles located at 135º and 315º respectively. The fifth result shows four 10 mm diameter bubble phantoms with their LBP image located at 45º, 135º, 225º and 315º respectively. The last one shows the image attained for a 10 mm electrode is located farther from the measurement electrode.

Table 2. Results of LBP.

Phantom	Reconstructed Image
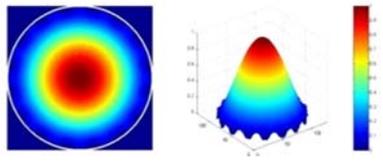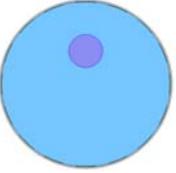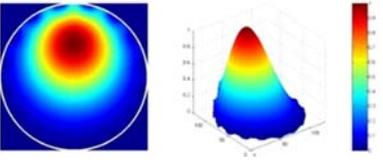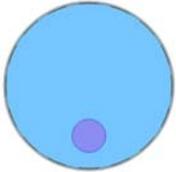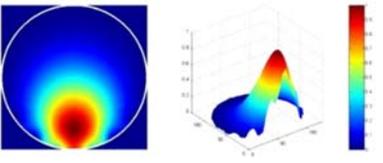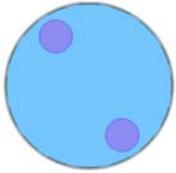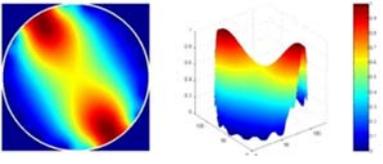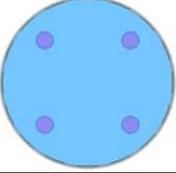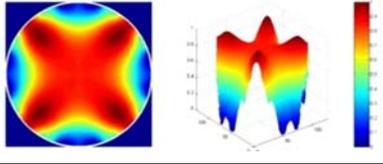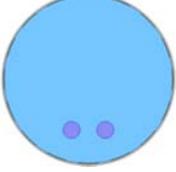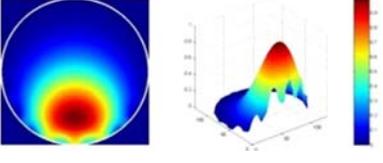
7. Conclusions

Linearization remains a widespread choice in ERT image reconstruction. Eventhough it could not provide an accurate image due to its linear approach; it does provide a fast on-line view for initial visualization. Generating a sensitivity distribution or also known as a sensitivity map of a homogeneous medium is a very important step in the linearization method. A correct sensitivity map is crucial in solving any inverse problems towards producing a correct image reconstruction. Upon solving the sensitivity distribution, the electrical potentials obtained will be fed to an inverse algorithm to obtain the previously unknown conductivity distribution. Simulation results of six bubble phantoms demonstrated that the invasive ERT sensor in a metal pipe applying conductivity boundary strategy together with the sensitivity based reconstruction algorithm is feasible to provide the cross sectional images of the water/gas two-phase flow. The locations of the bubbles can also be well distinguished. However, the exact shape of the conductivity distribution was not obtained due to the imperfection of the linear method approximations in the algorithm used since the method is linear and has fixed weighting factor.

Acknowledgements

References

[1]. Jin, H., Yang, S., He, G., Wang, M. and Williams, R. A., The effect of gas-liquid counter-current operation on gas hold-up in bubble columns using electrical resistance tomography, *Journal of Chemical Technology and Biotechnology*, 85, 9, 2010, pp. 1278-1283.

[2]. Xu, Y., Wang, H., Cui, Z. and Dong, F., Application of electrical resistance tomography for slug flow measurement in gas/liquid flow of horizontal pipe, *IEEE Computer Society*, 2009.

[3]. Dyakowski, T., Jeanmeure, L. F. C. and Jaworski, A. J., Applications of electrical tomography for gas–solids and liquid–solids flows — a review, *Powder Technology*, 112, 3, 2000, pp. 174-192.

[4]. Wang, M., Dickin, F. J. and Williams, R. A., Electrical resistance tomography of metal walled vessels and pipelines, *Electronics Letters*, 30, 10 1994, pp. 771-773.

[5]. Aw, S. R., Rahim, R. A., Rahiman, M. H. F., Yunus, F. R. M. and Goh, C. L., Electrical resistance tomography: A review of the application of conducting vessel walls, *Powder Technology*, 254, 2014, pp. 256-264.

[6]. Grieve, B. D., On-line Electrical Impedance Tomography for Industrial Batch Processing, *UMIST Manchester,* UK, 2002.

[7]. Davidson, J. L., Ruffino, L. S., Stephenson, D. R., Mann, R., Grieve, B. D. and York, T. A., Three-dimensional electrical impedance tomography applied to a metal-walled filtration test platform, *Measurement Science and Technology*, 15, 11 2004, p. 2263.

[8]. Fan, W. R. and Wang, H. X., Maximum entropy regularization method for electrical impedance tomography combined with a normalized sensitivity map, *Flow Measurement and Instrumentation*, 21, 3, 2010, pp. 277-283.

[9]. Seppanen, A., Karhunen, K., Lehikoinen, A., Kaipio, J. P. and Monteiro, P. J. M., Electrical resistance tomography imaging of concrete, *CRC Press,* 2009.

[10]. Yong Song, K. and et al., Sensitivity map generation in electrical capacitance tomography using mixed normalization models, *Measurement Science and Technology*, 18, 7, 2007, p. 2092.

[11]. Karhunen, K., Seppanen, A., Lehikoinen, A., Blunt, J., Kaipio, J. P. and Monteiro, P. J. M., Electrical resistance tomography for assessment of cracks in concrete, *ACI Materials Journal*, 107, 5 2010, pp. 523-531.

[12]. Wang, M., Dickin, F. J. and Mann, R., Electrical Resistance Tomographic Sensing Systems for Industrial Applications, *Chemical Engineering Communications*, 175, 1 1999, pp. 49-70.

[13]. Huang, S., Wang, Z. and Jin, Y., Studies on gas-solid-solid circulating fluidized-bed reactors, *Chemical Engineering Science*, 54, 13-14, 1999, pp. 2067-2075.

[14]. Lehr, J., A Vector Derivation Useful in Impedance Plethysmographic Field Calculations, *IEEE Transactions on Biomedical Engineering,* BME-19, 2, 1972, pp. 156 - 157.

[15]. Zhou, H., Xu, L., Cao, Z., Hu, J. and Liu, X., Image reconstruction for invasive ERT in vertical oil well logging, *Chinese Journal of Chemical Engineering*, 20, 2, 2012, pp. 319-328.

[16]. Sun, J. and Yang, W., Evaluation of fringe effect of electrical resistance tomography sensor. *Measurement*, 53, 2014, pp. 145-160.

[17]. Rasteiro, M. G., Silva, R., Garcia, F. A. P., Faia, P., Electrical Tomography: a review of Configurations and Applications to Particulate Processes, *KONA Powder and Particle Journal*, 29, 2011, pp. 67 - 80.

[18]. William, L., Nicholas, P. and Andrea, B., The reconstruction problem, *Taylor & Francis,* 2004.

[19]. Mohd Hafiz Fazalul Rahiman, Zulkarnay Zakaria, Ruzairi Abdul Rahim, Wei Nyap Ng, Ultrasonic tomography imaging simulation of two-phase homogeneous flow, *Emerald Sensor Review*, 29, 3 2009, pp. 266 - 276.

[20]. Z. Zakaria, R. Abdul Rahim, M. S. B Mansor, S. Yaacob, N. M. Nor Ayob, S. Z. Mohd. Muji, M. H. fazalul Rahiman, S. M. K. Syed Aman, Advancements in transmitters and sensors for biological tissue imaging in magnetic induction tomography, *Sensors,* 2012, 12, 6, pp. 7126-7156.

[21]. M. H. Fazalul Rahiman, R. Abdul Rahim and N. M. Nor Ayob, The Front-End Hardware Design Issue in Ultrasonic Tomography, *IEEE Sensor Journal,* Vol. 10, No. 7, pp. 1276 -1281.

_____